Morphological Confinement on Crystallization in Blends of Poly(oxyethylene-*block*-oxybutylene) and Poly(oxybutylene)

Jun-Ting Xu,† Simon C. Turner, J. Patrick A. Fairclough, Shao-Min Mai, and Anthony J. Ryan*

The Polymer Centre, Department of Chemistry, University of Sheffield, Sheffield S3 7HF, U.K.

Chiraporn Chaibundit and Colin Booth

Department of Chemistry, The University of Manchester, Manchester M13 9PL, U.K.

Received September 10, 2001; Revised Manuscript Received February 5, 2002

ABSTRACT: Three poly(oxyethylene-*block*-oxybutylene) diblock copolymers, $E_{76}B_{38}$, $E_{114}B_{56}$, and $E_{155}B_{76}$, were blended with poly(oxybutylene) homopolymer, B_{14} and B_{28}, such that lamellae (lam), gyroid (gyr), hexagonally packed cylinders (hex), and body-centered-cubic (bcc) spheres were obtained in the melt. The nonisothermal crystallization on cooling of the blends was investigated with synchrotron small-angle X-ray scattering (SAXS) and differential scanning calorimetry (DSC). In general, two classes of behavior are observed. In confined crystallization the morphology of the melt is retained, and crystals have limited dimensions. In breakout crystallization the melt morphology is destroyed, and a new lamellar morphology is formed. The morphological state (confinement in or breakout of melt morphology) during crystallization was evaluated by the change of the position of the first-order peak (q^*) in SAXS and the crystallization temperature (T_c). Breakout of morphology was observed in all $E_{76}B_{38}/B_{14}$ blends and $E_{114}B_{56}/B_{28}$ and $E_{155}B_{76}/B_{28}$ blends with lam morphology, while confined crystallization occurred in $E_{155}B_{76}/B_{28}$ blends with hex and bcc morphologies and $E_{114}B_{56}/B_{28}$ blends with bcc morphology. Confined crystallization was also observed in low E content $E_{114}B_{56}/B_{28}$ blends with hex morphology. These findings lead to two conclusions: (i) the tendency of confined crystallization varies with morphology and decreases in the order bcc > hex > lam, and (ii) confinement on crystallization tends to increase with the extent of segregation between the two blocks. The DSC results show that the crystallization temperature of the blends varies with morphology and chain length of the block copolymers. A much lower T_c was observed for the blends exhibiting confined crystallization behavior, and this phenomenon is explained by a homogeneous nucleation mechanism. The morphology over a larger scale was also examined by polarized light microscopy, and spherulite formation was only observed in the blends where the morphology was easily broken out during crystallization.

Introduction

The morphology of semicrystalline block copolymers has received increasing attention recently.[1] In a purely amorphous diblock copolymer, microphase separation is driven by incompatibility of the blocks, and morphology depends entirely on block copolymer structure. In contrast, the formation of morphology in a semicrystalline block copolymer is more complicated, since the crystallization process of one of the blocks competes with microphase separation.[2,3] There are two possibilities for the morphology of a semicrystalline diblock copolymer after crystallization: either the preexisting ordered mesophase of the melt is destroyed by crystallization or the crystallization is confined in the preexisting mesophase without morphological transformation. The final morphology of semicrystalline diblock copolymers depends on the thermal history and the nature of the blocks. For weakly segregated diblock copolymers, crystallization usually erases the ordered morphology in the melt when the other block is mobile (crystallization temperature is higher than glass transition temperature of the other block, $T_c > T_g$),[4−6] while confined crystallization is frequently observed at a lower crystallization temperature ($T_c < T_g$), where confinement is by hard (glassy) walls.[7−10] For strongly segregated block copolymers, even though the crystallization temperature is higher than the glass transition temperature of the noncrystallizable block, confined crystallization can still be observed.[11−13] Morphologies, such as lamellae (lam), gyroid (gyr), hexagonally packed cylinder (hex), and body-centered-cubic (bcc) sphere, can be formed in block copolymers, depending on the volume fractions of the two blocks, and these morphologies can lead to crystallization that is confined in different dimensions: lamellae are one-dimensionally confined, cylinders are two-dimensionally confined, and spheres are three-dimensionally confined. The difference in dimensionality of confinement may have a vital influence on the breakout of morphology. However, there are few reports on this so far. Recently, Chen et al. blended poly(1,4-butadiene) with poly(ethylene oxide)-*block*-poly(1,4-butadiene) (PEO-*b*-PB), a strongly segregated system, and found that the crystallization temperature of E block in the blends with hex and bcc morphologies was much lower than that in the blends with lam morphology.[14a] This is an indication of confined crystallization; direct evidence for limited confinement by SAXS and TEM was presented in a subsequent work.[14b] As the extent of segregation of the blocks must strongly affect the confinement of crystallization, we supposed that it would also be apparent in block copolymer/homopolymer blends. Zhu et al. reported both hard and soft confinement in the blends of polystyrene homopolymer (PS) with PEO-*b*-PS block copolymer, depending on the molecular weight of PS

† Permanent address: Department of Polymer Science & Engineering, Zhejiang University, Hangzhou 310027, China.

* To whom correspondence should be addressed.

10.1021/ma0116147 CCC: $22.00
Published on Web 03/29/2002

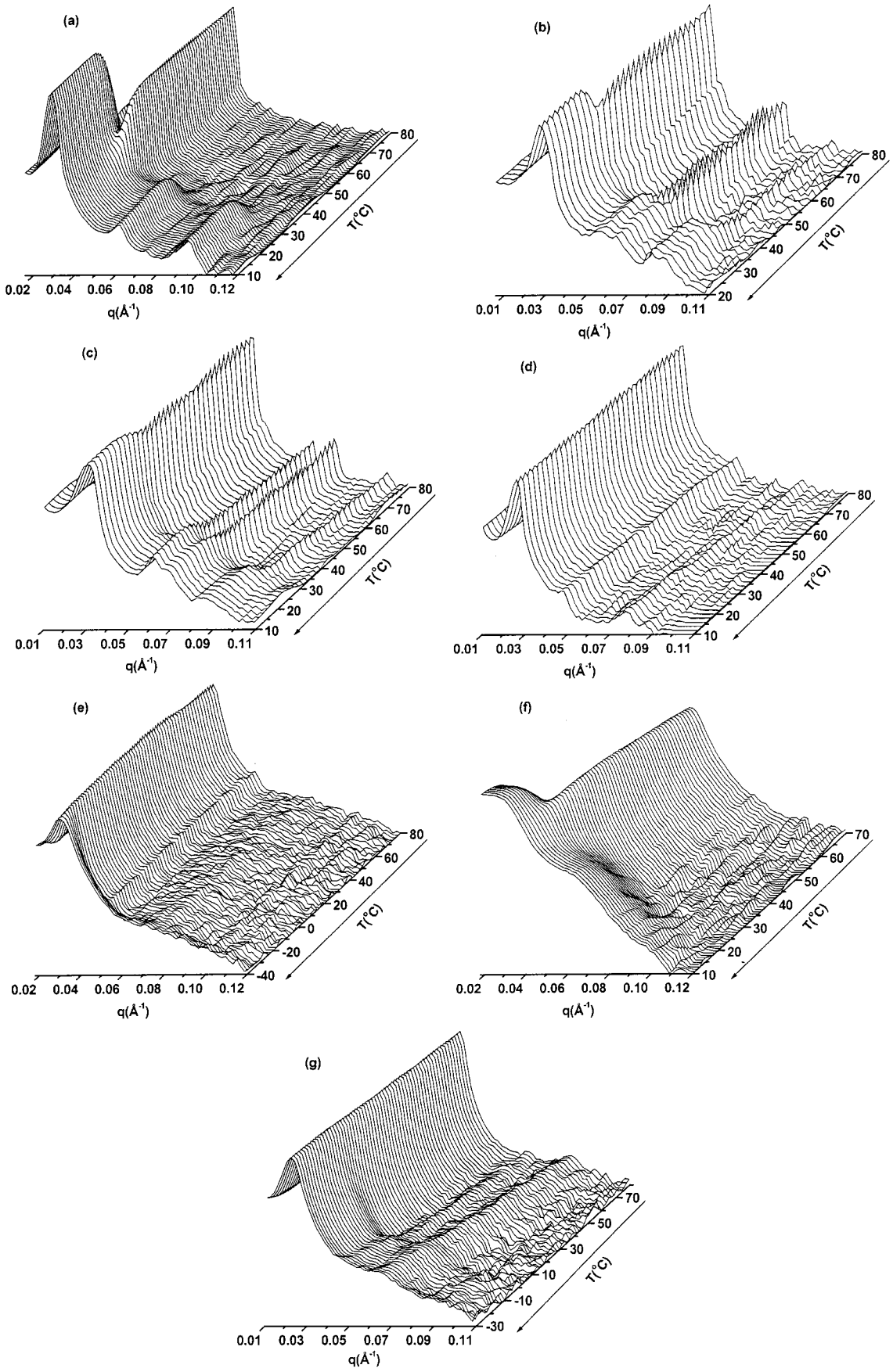

Figure 1. Three-dimensional SAXS profiles (log($I(q)$)) of selected blends. (a) $E_{114}B_{56}$, $\phi_B = 0.50$ (lam → lam); (b) $E_{114}B_{56}/B_{28}$, $\phi_B = 0.60$ (gyr → lam, mixed spacing lamellar morphology in the solid); (c) $E_{114}B_{56}/B_{28}$, $\phi_B = 0.70$ (hex → lam, mixed spacing lamellar morphology in the solid); (d) $E_{114}B_{56}/B_{28}$, $\phi_B = 0.76$ (hex → confined hex); (e) $E_{114}B_{56}/B_{28}$, $\phi_B = 0.83$ (bcc → confined bcc); (f) $E_{76}B_{38}/B_{14}$, $\phi_B = 0.83$ (bcc → lam); (g) $E_{155}B_{76}/B_{28}$, $\phi_B = 0.70$ (hex → confined hex). The changes of morphology before and after crystallization are indicated in the brackets.

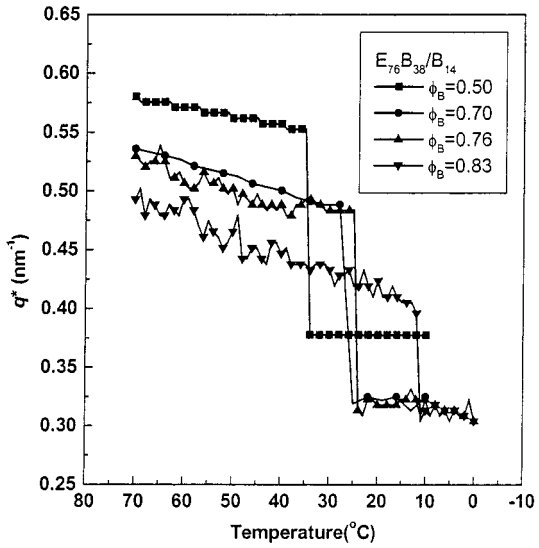

Figure 2. Change of q^* during crystallization for $E_{76}B_{38}/B_{14}$ blends.

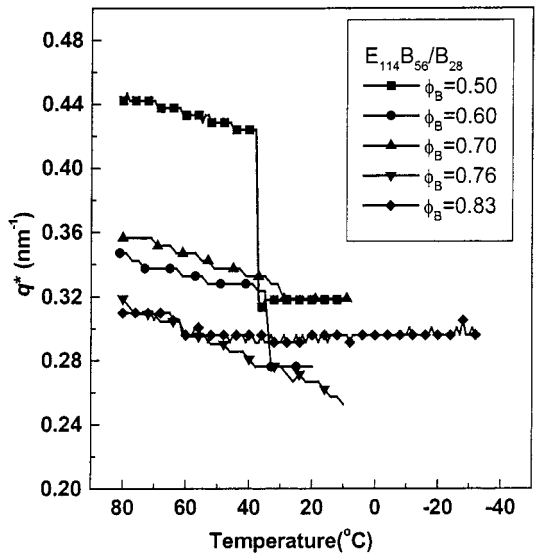

Figure 3. Change of q^* during crystallization for $E_{114}B_{56}/B_{28}$ blends.

homopolymer.[15] In the present work we selected three low-molecular-weight poly(oxyethylene-*block*-oxybutylene) copolymers with different chain length but similar volume fraction ($\phi_B \sim 0.5$), $E_{76}B_{38}$, $E_{114}B_{56}$, and $E_{155}B_{76}$, and blended them with poly(oxybutylene) in different proportions. In each morphology series the length of the crystallizable block is invariant, and the morphology is changed by dilution of the noncrystallizable block with its homopolymer. This allows the crystallization on cooling to be assessed without the complication of synthesizing a new molecule for each experiment or comparing molecules of varying length. The crystallization of poly(oxyethylene) segments in these blends was investigated using synchrotron small-angle X-ray scattering (SAXS) and differential scanning calorimetry (DSC).

Experimental Section

Materials. The synthesis and characterization of E_nB_m copolymers (where the subscripts refer to the average degree of polymerization) have been described elsewhere.[16,17] The homopolymers and block copolymers have narrow molecular

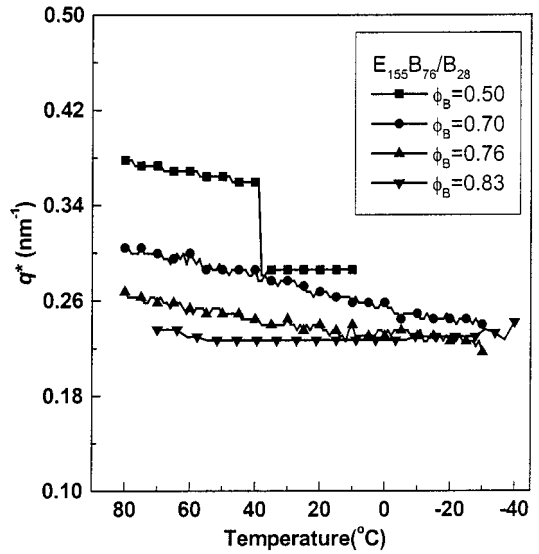

Figure 4. Change of q^* during crystallization for $E_{155}B_{76}/B_{28}$ blends.

Table 1. Oxyethylene/Oxybutylene Diblock Copolymers

copolymers	ϕ_E[a] (solid state)	w_E[b] (solid state)	ODT (°C)	liquid structure
$E_{76}B_{38}$	0.49	0.55	114	lam
$E_{114}B_{56}$	0.50	0.55	210	lam
$E_{155}B_{76}$	0.50	0.56	270	lam

[a] $\phi_E = n/[n + (72/44)(1.23/0.97)m]$, 1.23 g/cm^3 being the density of E in the crystalline state and 0.97 g/cm^3 the density of B in the liquid state, both at 20 °C. [b] $w_E = n/[n + (72/44)m]$.

weight distributions ($M_w/M_n < 1.05$) by GPC. The melt phase behavior of the block copolymers is summarized in Table 1. The PBO homopolymer with $M_n = 2000$ (B_{28}) was purchased from Aldrich and was used without further purification. The other PBO homopolymer with $M_n = 1000$ (B_{14}) was specially synthesized by anionic polymerization. Both have narrow molecular weight distributions.

Preparation of the Blends. The blends of E_nB_m with B_h were prepared by solution blending with dicholoromethane as solvent. To ensure that B homopolymer was miscible with B segments in block copolymers and the condition of "wet brush" was met,[18,19] the molecular weight of B homopolymer was smaller than half that of the B block. As a result, $E_{76}B_{38}$ was blended with B_{14}, and the other two block copolymers were blended with B_{28}. Following solvent evaporation, the blends were dried under vacuum for 24 h at 60 °C, then cooled to room temperature slowly, and stored below 0 °C for usage.

Time-Resolved Small-Angle X-ray Scattering. The simultaneous time-resolved SAXS/DSC experiments were carried out on beamlines 8.2 and 2.1 of the SRS at the Daresbury, Warrington, UK. The samples were cooled from 80 °C (70 °C for $E_{76}B_{38}$ and its blends) at a rate of 10 °C/min. The data were collected in 10 s frames separated by a waiting time of 10 μs. Details of the instrument and data processing are described elsewhere.[16,17]

DSC Measurements. Nonisothermal crystallization of the pure block copolymers and blends was performed on a Perkin-Elmer Pyris-1 calorimeter. Samples of the copolymer (about 5−10 mg, depending on PBO volume fraction in the blends) were sealed with aluminum pans and were heated to 80 °C (70 °C for $E_{76}B_{38}$ and its blends), held for 5 min, and then cooled at a rate of 5 °C/min until crystallization was completed. The peak temperature in the crystallization traces was taken as crystallization temperature (T_c) of the blends, and the data of T_c were presented with ignorance of the thermal lag.

Polarized Light Microscopy. Polarized light microscopy experiments were conducted on an Olympus BX50 microscope connected to a Panasonic NV-HD660 video recorder. Samples with ~1 μm thickness were heated to 80 °C and held for

Table 2. Domain Sizes of Different E_nB_m/B_h Blends in the Melt and Solid

block copolymers	ϕ_B[a] 70 °C	ϕ_B[a] solid	morphology change	*d*-spacing (Å) 70 °C	*d*-spacing (Å) after T_c	R[b] (Å) 70 °C	R[b] (Å) after T_c	L[c] (Å) 70 °C	N_E[d] 70 °C	stems of E[e] after T_c	T_m[f] (°C)
$E_{76}B_{38}$	0.48	0.49	lam → lam	108	167	28	42	52	1.8×10^{14}	2.6	56.3
	0.74	0.76	hex → lam	119	198	37	24	63	2.3×10^{16}	4.5	48.0
	0.82	0.83	bcc → lam	128	207	50	18	57	1.9×10^{18}	6.0	47.6
$E_{114}B_{56}$	0.48	0.50	lam → lam	142	198	37	50	68	1.4×10^{14}	3.2	55.0
	0.74	0.76	hex → hex	203	249	63	74	108	8.0×10^{15}	2.2	53.9
	0.82	0.83	bcc → bcc	206	203	81	78	90	4.5×10^{17}	2.1	54.6
$E_{155}B_{76}$	0.48	0.50	lam → lam	168	220	44	55	80	1.1×10^{14}	4.0	56.0
	0.74	0.76	hex → hex	243	273	75	81	130	5.6×10^{15}	2.7	55.6
	0.82	0.83	bcc → bcc	267	270	105	104	117	2.0×10^{17}	2.1	53.7

[a] The densities of E and B at 70 °C are 1.067 and 0.923 g/cm^3, respectively.[17] For the densities of E and B in solid see Table 1. [b] Half thickness of E domain for lam morphology ($R = d\phi_E/2$) or radius for hex ($R = d[2\phi_E/\sqrt{3}\pi)]^{1/2}$) and bcc ($R = d[3\sqrt{2}\phi_E/(4\pi)]^{1/3}$) morphologies, calculated based on volume fraction and geometry.[33] [c] Distance between two nearest E domains ($L = d - 2R$ for lam morphology, $L = 2d/\sqrt{3} - 2R$ for hex morphology, and $L = \sqrt{6}d/2 - 2R$ for bcc morphology[33]). [d] The number of E domains per cm^3, calculated based on the assumption that the length of cylinders and the length and height of lamellae are all 1 μm. [e] The average number of E stems per chain in crystals was calculated by $l/2R$ ($l = 2.85m$ Å, m and 2.85 Å being the number of E units in block copolymers and the length of a E unit in crystal with helical conformation, respectively). [f] Cooling rate is 5 °C/min, and heating rate is 10 °C/min.

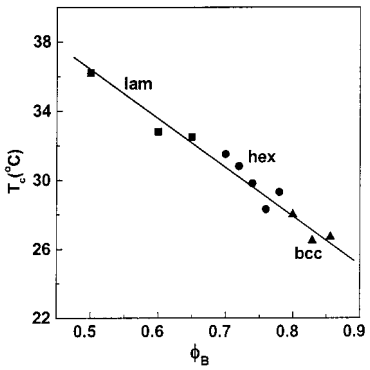

Figure 5. Plot of crystallization temperature (T_c) vs PBO volume fraction (ϕ_B) for $E_{76}B_{38}/B_{14}$ blends.

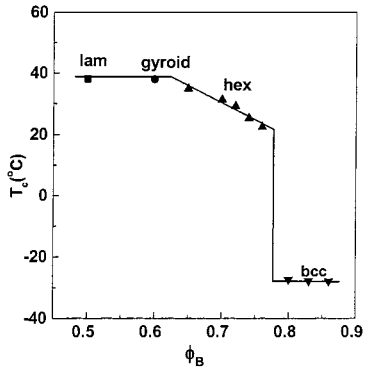

Figure 6. Plot of crystallization temperature (T_c) vs PBO volume fraction (ϕ_B) for $E_{114}B_{56}/B_{28}$ blends.

5 min using a Linkam DSC equipped with a liquid N_2 cooling system. Subsequently, the samples were cooled at a rate of 5 °C/min, and the texture of the blends during crystallization was recorded.

Results and Discussion

SAXS Results. The three-dimensional SAXS profiles ($\log(I(q))$) of selected $E_{114}B_{56}/B_{28}$, $E_{76}B_{38}/B_{14}$, and $E_{155}B_{76}/B_{28}$ blends cooled from the melt are shown in Figure 1. The pure $E_{114}B_{56}$ block copolymer has a lamellar morphology (Figure 1a). When it is cooled from the ordered melt, a significant displacement of the first-order peak is observed upon crystallization. Similar behavior occurs in the blends of $E_{114}B_{56}/B_{28}$ with $\phi_B = 0.60$ and 0.70, which have gyroid and hex morphologies in the melt but lamellar morphology after crystallization (Figure 1, b and c), respectively, but the displacement of the first

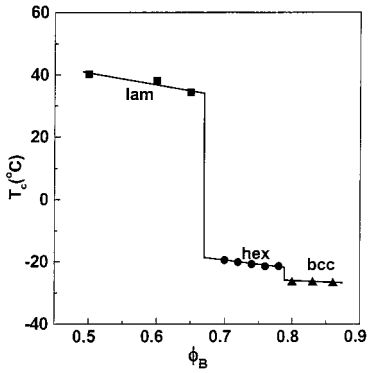

Figure 7. Plot of crystallization temperature (T_c) vs PBO volume fraction (ϕ_B) for $E_{155}B_{76}/B_{28}$ blends.

peak becomes smaller as the volume fraction of PBO increases. These observations indicate that crystallization leads to breakout morphology in these three samples. The two-dimensional SAXS profiles (not shown here) can give a clearer insight into the breakout of the morphology. A new peak appears at lower q^* value at the beginning of crystallization. The intensity of this peak increases gradually as the progress of crystallization, and at last it overwhelms the original peak in the ordered melt. In the contrast, the $E_{114}B_{56}/B_{28}$ blends with $\phi_B = 0.76$ and 0.83 (Figure 1, d and e), having hex and bcc morphologies, respectively, exhibit no appreciable displacement in the first-order peak after crystallization, and the higher-order reflections from the nonlamellar morphology imply confined crystallization. For $E_{76}B_{38}/B_{14}$ blends, the morphology broke out after crystallization in all the blends, and no confinement in crystallization was observed, even in the blend of high PBO volume fraction, such as the blend with $\phi_B = 0.83$ (bcc morphology) (Figure 1f). Furthermore, for $E_{155}B_{76}/B_{28}$ blends the displacement of the first-order peak is not observed in the blend with $\phi_B = 0.70$ (Figure 1g). Overall, the results indicate that confined crystallization occurs at a lower PBO volume fraction in $E_{155}B_{76}/B_{28}$ blends than in $E_{114}B_{56}/B_{28}$ blends and not at all in $E_{76}B_{38}/B_{14}$ blends.

One of the ways that breakout or confined crystallization can be determined is from the change in q^* and higher-order reflections. If the value of q^* shows a step change on crystallization, the morphology has broken out from the original melt structure to form lamellae; otherwise, if q^* changes smoothly through crystallization (and the higher-order reflections from the original

melt structure are retained), it is confined. Figures 2, 3, and 4 summarize the changes of q^* in the crystallization process for $E_{76}B_{38}/B_{14}$, $E_{114}B_{56}/B_{28}$, and $E_{155}B_{76}/B_{28}$ blends, respectively. A step change in q^* is observed in all $E_{76}B_{38}/B_{14}$ blends, irrespective of the morphology, indicating breakout crystallization in all these blends. The $E_{114}B_{56}/B_{28}$ blends with lamellar and gyroid morphologies and some (higher E fraction) blends with hex morphology also exhibit a step change in q^*, but q^* changes continuously in other blends with hex morphology and all the blends with bcc morphology. These findings reveal that, for $E_{114}B_{56}/B_{28}$ blends, confined crystallization occurs in the blends with bcc morphology and some blends with hex morphology, but the morphology breaks out in the blends with lamellar and gyroid morphologies and in blends of hex morphology with high ϕ_E. In the $E_{155}B_{76}/B_{28}$ blends, a step change of q^* was observed only in the blends with lamellar morphology, whereas all the $E_{155}B_{76}/B_{28}$ blends with hex and bcc morphologies exhibited confined crystallization.

One can see from Figure 1 that only lamellar morphology is formed in the solid after the morphology has broken out upon crystallization, irrespective of the original morphology in the melt, while the morphology in the melt is retained in the solid in the case of confined crystallization. Breakout or confinement of crystallization also leads to changes in the higher-order SAXS peaks. The higher-order reflections of the lamellar morphology are strong after morphological breakout, and lamellar stacks have been formed under slow growth conditions following rearrangement of the melt. In contrast, the higher-order reflections are often reduced in intensity and sometimes disappear after confined crystallization, as the original lattice becomes somewhat distorted and the minority domains become deformed to accommodate the change in volume on crystallization.[20]

Crystallization Temperature. The peak crystallization temperature (T_c) of different blends is plotted vs B volume fraction in Figures 5−7. Comparing these figures, one can see that the three types of blends show remarkable difference in $T_c-\phi_B$ profiles. The crystallization temperature of $E_{76}B_{38}/B_{14}$ blends (Figure 5) decreases gradually from 36 to 26 °C with increasing ϕ_B. For $E_{114}B_{56}/B_{28}$ blends (Figure 6), the variation of crystallization temperature with B volume fraction can be divided into three regimes according to the morphology of the blends. The blends with lamellar and gyroid morphologies show similar crystallization temperatures, while the blends with hex morphology show the crystallization temperature decreasing as PBO volume fraction is increased. When the morphology of the blends transforms to bcc, the crystallization temperature exhibits a marked drop, and it is much lower than that of the blends with hex morphology. All the blends with bcc morphology have similar crystallization temperature. Two stepwise regimes are observed for the crystallization temperature of $E_{155}B_{76}/B_{28}$ blends (Figure 7) where all blends with the same type of morphology have similar crystallization temperatures. The crystallization temperatures of the blends having hex and bcc morphologies are much lower than those of the blends with lamellar morphology. Similar DSC experiments have carried out for a strongly segregated system, PEO-*b*-PB/PB blends, by Chen et al.,[14] and they obtained a $T_c-\phi_B$ profile similar to that of $E_{155}B_{78}/B_{28}$ (Figure 7). The present results show that a two-regime profile is just one of several possible types of profile, which depend on the extent of segregation of the blocks.

The crystallization temperature of the blends can be viewed as an indication of confined crystallization or breakout of the morphology in the crystallization process. If the morphology breaks out, this means that different E domains in the blends can communicate each other, and only few nuclei are needed for crystallization.[20] By contrast, if crystallization is confined, crystallization in one domain cannot spread into another domain, and at least one nucleus is needed for each E domain to ensure complete crystallization of the PEO. Since the E domains in block copolymers, especially hex and bcc domains, are far smaller than spherulites,[14] the number of nuclei needed in confined crystallization is much larger than that in nonconfined crystallization, and the primary nucleation process becomes the rate-determining step in confined crystallization. In fact, it is generally believed that confined crystallization follows a homogeneous nucleation mechanism,[20−23] since the number of impurities, which act as heterogeneous nuclei, is very small when compared to the number of E domains, and the E fraction initiated by heterogeneous nucleation accounts for only a very minor part of the crystallizable material. For example, the number of E domains/cm^3 is of order 10^{14}, 10^{15}, and 10^{17} for the blends with lam, hex, and bcc morphology, respectively, if we assume that the length of cylinders, the length, and width of lamellae are all 1 μm. By contrast, the number of impurities is estimated to be only of order 10^5 when it is assumed that one impurity initiates only one spherulite, and the radius of the spherulites formed is 100 μm (see Table 2). The relationship between homogeneous nucleation rate and temperature can be expressed by following equation:[24]

$$V_{nuc} \sim \exp\left(-\frac{(\text{const})\sigma^3 {v_m}^2 (T_f^\infty)^2}{kT_c(\Delta {H_m}^f)^2(T_f^\infty - T_c)^2}\right) \qquad (1)$$

where V_{nuc} is the rate of homogeneous nucleation, $\Delta {H_m}^f$ and σ denote the heat of fusion per chain unit and the excess free energy per unit area of the surface of the nucleus, respectively, v_m designates the volume of a chain unit, and T_f^∞ is the equilibrium melting temperature of the polymer.

According to eq 1, the homogeneous nucleation rate monotonically increases with supercooling ΔT ($\Delta T = T_f^\infty - T_c$) when ΔT is between 0 and $^2/_3$ T_f^∞ (for PEO, it is from 0 to ~230 K). Since the nonisothermal experiment was conducted in the present work and the blends were cooled at a fast rate in similar temperature ranges, both breakout crystallization and confined crystallization are completed in the similar time scale (but not at similar temperatures) and thus have similar crystallization rates. This is supported by the fact of similar crystallization curves in both types of crystallization. To maintain a crystallization rate comparable to that in nonconfined crystallization, the crystallization temperature should be much lower for the confined crystallization to produce one nucleus per domain on the same time scale. The above analysis shows that large supercooling for crystallization is the cooperative result of confinement and homogeneous nucleation. This point is important for understanding the confined crystallization behavior in block copolymers, since confinement and homogeneous nucleation are correlated, as has been shown for confinement by a glassy block.[25]

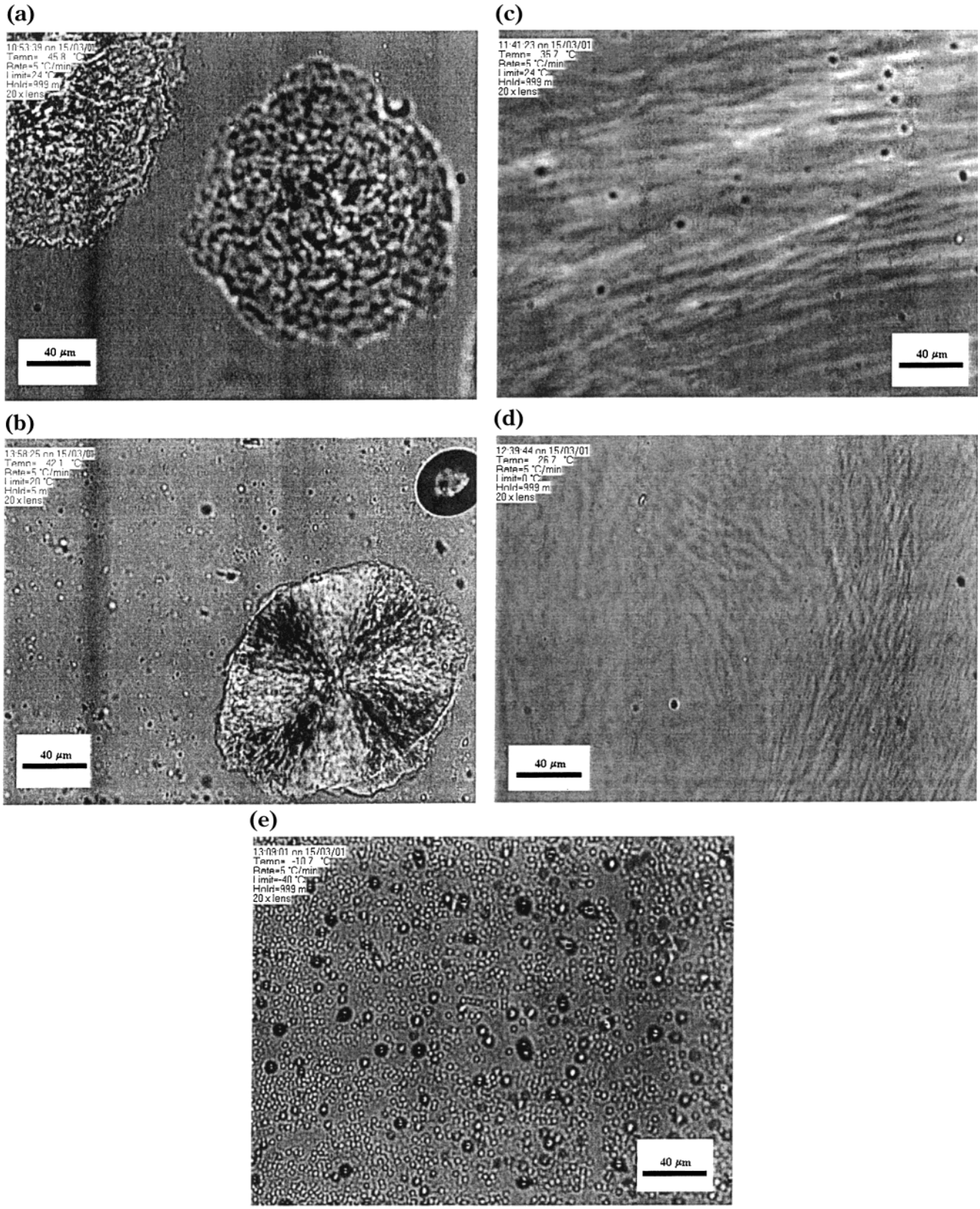

Figure 8. PLM micrographs of $E_{114}B_{56}$/PBO blends during crystallization: (a) $\phi_B = 0.50$, (b) $\phi_B = 0.60$, (c) $\phi_B = 0.70$, (d) $\phi_B = 0.76$, and (e) $\phi_B = 0.83$.

The SAXS and DSC results have clearly revealed the crystallization behavior of E_nB_m/B_h blends varies with morphology and chain length of the block copolymers. These findings lead to the conclusion that the ability to confine crystallization increases in the order lam (gyroid) < hex < bcc. There are two possible reasons for this. First, the bcc morphology is three-dimensionally confined, hex morphology is two-dimensionally confined, and lamellar morphology is only one-dimensionally confined. In fact, a high fraction of lamellar domains are not confined but interconnected due to screw dislocations.[26,27] The grain boundaries in hexagonal

block copolymer melts tend to separate the minority rods[1] and reduce the connectivity of the crystallizable material, and obviously grain boundaries in spherical systems also separate minority domains. Since one-dimensional breakout is always easier than three-dimensional breakout, confined crystallization occurs most frequently in bcc morphology. Second, when the morphology changes from lam to hex and to bcc, the *d*-spacing increases accordingly. The data in Table 2 show that the distance between two nearest E domains (L) is relatively small in all $E_{76}B_{38}/B_{14}$ blends but correspondingly larger for the $E_{114}B_{56}/B_{28}$ and $E_{155}B_{76}/B_{28}$ blends. The larger *d*-spacing means more interactions between E and B segments during morphological breakout, which is unfavorable in energy and results in larger barrier to mass transport. If we estimate the diffusion coefficient to go with $D \propto M^{-2}$, this increases the effect for the longer copolymers. That is the diffusion time for rearrangement which scales as d^2 takes on a stronger dependence with molecular weight with $t \propto d^2M^2$.[28] Moreover, the chain length of the diblock copolymers used for blending has a second important effect on the morphological breakout or confinement. For the blends containing shorter diblock copolymer $E_{76}B_{38}$, no confined crystallization is observed, while for the blends of $E_{155}B_{78}$ confined crystallization starts from a lower PBO fraction. The longer the diblock polymer chain means larger χN and stronger incompatibility between E and B segments, which leads to a larger energy barrier during the breakout of morphology. Thus, we reach the conclusion that crystallization is confined more easily as the extent of segregation of the blocks is increased.

Morphology Observed by PLM. The morphology of the blends was also observed by polarized light microscopy (PLM), and selected micrographs of $E_{114}B_{56}/B_{28}$ blends are shown in Figure 8. Coarse spherulite morphology without obvious Maltese crosses was observed for the pure $E_{114}B_{56}$ block copolymer (Figure 8a). In contrast, addition of a small amount of PBO ($\phi_B = 0.60$) to the block copolymer leads to well-defined spherulites with clear Maltese crosses (Figure 8b). The appearance of spherulites is strong evidence of breakout from the lamellae and gyroid morphologies in these two samples because the formation of spherulites needs the reorganization of different E domains.[29,30] The $E_{114}B_{56}/B_{28}$ blends with $\phi_B = 0.70$ and $\phi_B = 0.76$ exhibit a fibril morphology (Figure 8, c and d). The disappearance of the spherulite morphology in these two blends indicates that the mobility of E is not high enough to form spherulites. The fibrils are of large length scale and could well be corrugations introduced by the volume change on crystallization. In the $E_{114}B_{56}/B_{28}$ blend with $\phi_B = 0.83$ (Figure 8e), it is found that spherical domains are scattered in the matrix. It should be noted that such morphology may also be artifactual, since this blend crystallizes at a very low temperature (see Figure 6), and the possibility that the observed spherical domains are condensed water vapor cannot be excluded, even though dry nitrogen was used to blanket the sample during experiments. What is readily apparent, though, is the absence of spherulites.

Conclusions

The SAXS and DSC studies show that E_nB_m/B_h blends exhibit either breakout or confined crystallization, which can be identified by changes in scattering vector (q^*) and crystallization temperature (T_c). In confined crystallization the blends have low T_c but no step change in q^*, the morphology of the melt being retained in the solid, while in breakout of crystallization a step change of q^* and a higher T_c are observed, the morphology in the melt being erased in favor of lamellar morphology in the solid. The occurrence of breakout or confined crystallization strongly depends on the original morphology in the melt. The ability of confining crystallization increases in the order lam < hex < bcc, possibly due to the differences in interconnectivity among and distance between E domains. The block lengths of the copolymers also influence the crystallization behavior of the blends. Longer diblock copolymer chains have larger incompatibility between E and B segments and are more strongly confined on crystallization, leading to the occurrence of confined crystallization at moderate PBO volume fractions. The present work reports crystallization of blends containing block copolymers; however, the homopolymer added to control the morphology (through the volume fraction) is noncrystalline, and all the crystallization occurs in domains comprising tethered chains. We believe, therefore, that the observed behavior and the conclusions we derive also apply to neat block copolymer systems, since similar crystallization kinetics have been found in both blends and pure block copolymers.[31,32]

Acknowledgment. J.X. was supported by The Board of Pao Yu-kong and Pao Zhao-long Scholarship during his stay at the University of Sheffield, S.M.M. and S.C.T. were supported by EPSRC Grants GR/L22621 and GR/M22116, respectively. Beamtime at Daresbury was provided under EPSRC Grant GR/M22116. Detailed discussions with R. A. Register aided our interpretation of the data and preparation of the manuscript.

References and Notes

(1) Hamley, I. W. *The Physics of Block Copolymers*; Oxford University Press: New York, 1998.
(2) DiMarzio, E. A.; Guttman, C. M.; Hoffmann, J. D. *Macromolecules* **1980**, *13*, 1194.
(3) Whitmore, M. D.; Noolandi, J. *Macromolecules* **1988**, *21*, 1482.
(4) Nojima, S.; Kato, K.; Yamamoto, S.; Ashida, T. *Macromolecules* **1992**, *25*, 2237.
(5) Rangarajan, P.; Register, R. A.; Fetters, L. J.; Bras, W.; Naylor, S.; Ryan, A. J. *Macromolecules* **1995**, *28*, 4932.
(6) Ryan, A. J.; Hamley, I. W.; Bras, W.; Bates, F. S. *Macromolecules* **1995**, *28*, 3860.
(7) Cohen, R. E.; Cheng, P. L.; Douzinas, K.; Kofinas, P.; Berney, C. V. *Macromolecules* **1990**, *23*, 324.
(8) Sakurai, K.; MacKnight, W. J.; Lohse, D. J.; Schulz, D. N.; Sissano, J. A.; Lin, J. S.; Agamalyan, M. *Polymer* **1996**, *37*, 4443.
(9) Zhu, L.; Chen, Y.; Zhang, A. Q.; Calhoun, B. H.; Chun, M. S.; Quirk, R. P.; Cheng, S. Z. D.; Hsiao, B. S.; Yeh, F. J.; Hashimoto, T. *Phys. Rev. B: Condens. Matter* **1999**, *60*, 10022.
(10) Zhu, L.; Cheng, S. Z. D.; Calhoun, B. H.; Ge, Q.; Quirk, R. P.; Hsiao, B. S.; Yeh, F. J. *Chin. J. Polym. Sci.* **2000**, *18*, 287.
(11) Quiram, D. J.; Register, R. A.; Marchand, G. R. *Macromolecules* **1997**, *30*, 4551.
(12) Quiram, D. J.; Register, R. A.; Marchand, G. R.; Ryan, A. J. *Macromolecules* **1997**, *30*, 8338.
(13) Rangarajan, P.; Register, R. A.; Adamson, D. H.; Fetters, L. J.; Bras, W.; Naylor, S.; Ryan, A. J. *Macromolecules* **1995**, *28*, 1422.
(14) (a) Chen, H. L.; Hsiao, S. C.; Lin, T. L.; Yamauchi, K.; Hasegawa, H.; Hashimoto, T. *Macromolecules* **2001**, *34*, 671. (b) Chen, H. L.; Wu, J. C.; Lin, T. L.; Lin, J. S. *Macromolecules* **2001**, *34*, 6936.
(15) Zhu, L.; Mimnaugh, B. R.; Ge, Q.; Quirk, R. P.; Cheng, S. Z. D.; Thomas, E. L.; Lotz, B.; Hsiao, B. S.; Yeh, F.; Liu, L. Z. *Polymer* **2001**, *42*, 9121.

(16) Mai, S. M.; Fairclough, J. P. A.; Viras, K.; Gorry, P. A.; Hamley, I. W.; Ryan, A. J.; Booth, C. *Macromolecules* **1997**, *30*, 8392.
(17) Mai, S. M.; Fairclough, J. P. A.; Terrill, N. J.; Turner, S. C.; Hamley, I. W.; Matsen, M. W.; Ryan, A. J.; Booth, C. *Macromolecules* **1998**, *31*, 8110.
(18) Tanaka, H.; Hasegawa, H.; Hashimoto, T. *Macromolecules* **1991**, *24*, 240.
(19) Winey, K. I.; Thomas, E. L.; Fetters, L. J. *Macromolecules* **1992**, *25*, 2645.
(20) Loo, Y. L.; Register, R. A.; Ryan, A. J. *Phys. Rev. Lett.* **2000**, *84*, 4120.
(21) Lotz, B.; Kovacs, A. J. *ACS Polym. Prepr.* **1969**, *10*, 820.
(22) Robitaille, C.; Prudhomme, J. *Macromolecules* **1983**, *16*, 665.
(23) Weimann, P. A.; Hajduk, D. A.; Chu, C.; Chaffin, K. A.; Brodil, J. C.; Bates, F. S. *J. Polym. Sci., Part B: Polym. Phys.* **1999**, *37*, 2053.
(24) Strobl, G. R. *The Physics of Polymers: Concepts for Understanding Their Microstructures and Behavior*, 2nd ed.; Springer: Berlin, 1997.
(25) Loo, Y. L.; Register, R. A.; Ryan, A. J.; Dee, G. T. *Macromolecules* **2001**, *34*, 8968.
(26) Hong, S.; MacKnight, W. J.; Russell, T. P.; Gido, S. P. *Macromolecules* **2001**, *34*, 2876.
(27) Hong, S.; MacKnight, W. J.; Russell, T. P.; Gido, S. P. *Macromolecules* **2001**, *34*, 2398.
(28) De Gennes, P. G. *Scaling Concepts in Polymer Physics*; Cornell University Press: Ithaca, NY, 1979.
(29) Floudas, G.; Tsitsilianis, C. *Macromolecules* **1997**, *30*, 4381.
(30) Liu, L. Z.; Li, H.; Jiang, B. Z.; Zhou, E. L. *Polymer* **1994**, *35*, 5511.
(31) Xu, J. T.; Fairclough, J. P. A.; Mai, S. M.; Ryan, A. J.; Chaibundit, C.; Booth, C. Manuscript in preparation.
(32) Loo, Y. L.; Register, R. A.; Ryan, A. J. *Macromolecules* **2002**, *35*, 2365.
(33) Shibayama, M.; Hashimoto, T.; Kawai, H. *Macromolecules* **1983**, *16*, 16.

MA0116147